Materials Research. 2018; 21(3): e20170545
DOI: http://dx.doi.org/10.1590/1980-5373-MR-2017-0545

Structural, optical and electrical properties of Ni-doped Co_3O_4 prepared via Sol-Gel technique

Abdelhak Lakehal[a,b]*, Benrabah Bedhiaf[a], Amar Bouaza[a], Hadj Benhebal[a], Abdelkader Ammari[a,c], Cherifa Dalache[d]

[a]*Laboratory of Physical Engineering, Ibn-Khaldoun University, Zaaroura, 14000, Tiaret, Algeria*
[b]*Synthesis and Catalysis Laboratory, Ibn-Khaldoun University, Zaaroura, 14000, Tiaret, Algeria*
[c]*Laboratory of Storage and Valorization of Renewable Energy, USTHB, el Alia 16111 Babezzouar Algiers, Algeria*
[d]*Department of Physics, Ibn Khaldoun University, Zaaroura, 14000, Tiaret, Algeria*

Received: June 03, 2017; Revised: December 13, 2017; Accepted: January 18, 2018

In this article, Nickel doped Cobalt oxide thin films and powders have been prepared on glass substrates using sol gel based dip coating process in order to investigate their optical, structural and electrical properties. The Ni concentration was changed from 0 to 9 wt(%).The synthesized samples were characterised by Ultraviolete visible analysis, X-ray diffraction, Fourier transform infrared spectroscopy and Complex impedance spectroscopy to depict the optical, structural, vibrational and electrical properties. Our structural results show that the obtained samples were composed of (Co_3O_4) polycrystalline with spinel-type preferentially oriented in the (311) plane. Our optical results show that the films have high transparency over the visible region (85% for Co_3O_4 and ~ 60-75% for all doped samples). The optical band gaps were found to be (E_{g1} = 1.50 *eV*, E_{g2} = 2.20 *eV*) and (E_{g1} = 1.42 *eV*, E_{g2} = 2.07 *eV*) for the case of (pure Co_3O_4 and 9% Ni-doped Co_3O_4) respectively. The complementary phase information is provided by FT-IR spectroscopy. FT-IR spectra confirms the presence of Co^{2+}-O and Co^{3+}-O vibrations in the spinel lattice. The Nyquist plots suggests that the equivalent circuit of our films is an parallel circuit R_pC_p. It was found that the resistance *Rp* decreases whereas the capacity *Cp* increases with increasing doping levels.

Keywords: *Cobalt oxide, Ni-doping, Sol-gel dip coating, Thin films.*

1. Introduction

In the last decade, transparent conductive oxides (TCO) have gained considerable interest in the research community due to their intriguing properties, they combine electrical conductivity and optical transparency in the visible range. These properties have attracted the attention for using them in optoelectronic devices such as photovoltaic solar cells, electrochromic sensor[1,2].

Among the transparent conductive oxides (TCO), cobalt oxide (Co_3O_4) is one of the most studied oxides due to its importance for various scientific fields[1] such as supercapacitors[3], solar selective absorber[4], and energy storage owing to its electrochemical stability[1], large surface area[4], and high conductivity. It is also characterized by good resistance to thermal shocks, oxidation, UV radiation, humidity and corrosion. Co_3O_4 exhibits p-type semiconducting property and behaves like an antiferromagnet (AF) with the Néel temperature $T_N \approx 290\ K$[5], Optical studies have shown that Co_3O_4 exhibits multiple direct band gap energies (E_{g1} = 1.48 *eV*, E_{g2} = 2.24 *eV*)[6]. It has three well-known valence states, the cobaltous oxide (CoO), the cobaltic oxide (Co_2O_3), and the cobalt cobaltite (Co_3O_4)[7]. The most stable phase in the cobalt oxide system is a mixed valence compound [$Co^{2+}Co^{3+}{}_2O_4$] with a normal spinel structure[3].

In recent years, several efforts have been devoted to fabricating nanostructured systems of cobalt oxide with tunable physical-chemical properties for broad range of applications, among which transition metal doping is a promising and efficient route to improve the optical absorption and the electrical behavior of Co_3O_4. In this regard, this study fabricates Ni-doped Co_3O_4 thin films in an effort to understand their enhanced optical and electrical properties. In our work, we choose doping by nickel because its atomic radius is almost equal to that of cobalt. A small change in doping concentration is significant for changing the band gaps, the energy band gaps are expected to vary in a wide and very attractive energies intervals.

Various routes of synthesis of Co_3O_4 films have been undertaken such as chemical vapor deposition[8], spray pyrolysis[9], sol-gel method[8,10,11], metal organic chemical vapor deposition (MOCVD)[12]. In this paper we have adopted a simple sol gel dip-coating method, this method of preparing

---

*e-mail: labdelhak91@outlook.fr

thin films has several advantages: its low cost, flexibility in the deposition process, and it is convenient for a large area and it can produce homogeneous thin films with very regular crystallites sizes[13-15]. It has been used successfully in our laboratory to fabricate a variety of porous materials such as SnO_2 [9], TiO_2 [16].

2. Experimental Details

2.1. Films and Powders preparation

In the present venture, a sol gel dip-coating setup operating at atmospheric pressure was used to deposit Ni-doped cobalt oxide thin films on glass substrates. To prepare 0.1 M solution of pure Co_3O_4, hexahydrate nitrate cobalt ($Co(NO_3)_2.6H_2O$) was dissolved in an aqueous solution of citric acid ($C_6H_8O_7$ total solutions volume was 30 ml) (citric acid can also act as an effective chelating agent to produce fine particles) and the resulting solution was stirred and heated at 80°C for 2 hours in order to obtain the burgundy homogeneous solution which is further converted into thick gel. The stoichiometric equilibrium reaction between the cobalt nitrate and citric acide used in this study,can be described by the following equation:

$$27\,Co(NO_3)_2 * 6\,H_2O + 14\,C_6H_8O_7 * H_2O \xrightarrow{Heat} 9\,Co_3O_4 + 27\,N_2\uparrow + 232\,H_2O + 84\,CO_2\uparrow$$

To achieve Ni-doping$\left\{\frac{[Ni]}{[Co]}\right\}$, nickel nitrate was added to the precursor solution with different concentrations (3 wt%, 5 wt%, 7 wt% and 9 wt%) for all doped samples. This mixture was equally stirred and heated at 80 °C for 2 hours to obtain viscous solution. The obtained viscous gel was calcined in muffle furnace at 400°C for 3 hours in a static air atmosphere to obtain Ni-doped Co_3O_4 powders. A schematic representation of the sol gel synthesis is given in Fig.1.

2.2. Film deposition

The procedure of cleaning glass substrates is very important to get well adherent, smooth films. The substrates Pyrex pieces (75 x 25 x1mm^3) were cleaned through dipping them in ultrasonic bath containing trichloroethylene, ethanol, aciton for 5 minutes respectively, and finally rinsed by distilled water. The substrates were dipped in the solution, The withdrawal speed of the substrates from the solution was 5Cm/min. The optimized deposition conditions are listed in Table 1. After coating process was completed, the films were heated at 100°C for 2 hours in the ambient to evaporate the solvent and then annealed at 400°C during 45 minutes to remove organic residues and for densification. The obtained samples were subjected to microstructural, optical and electrical analysis.

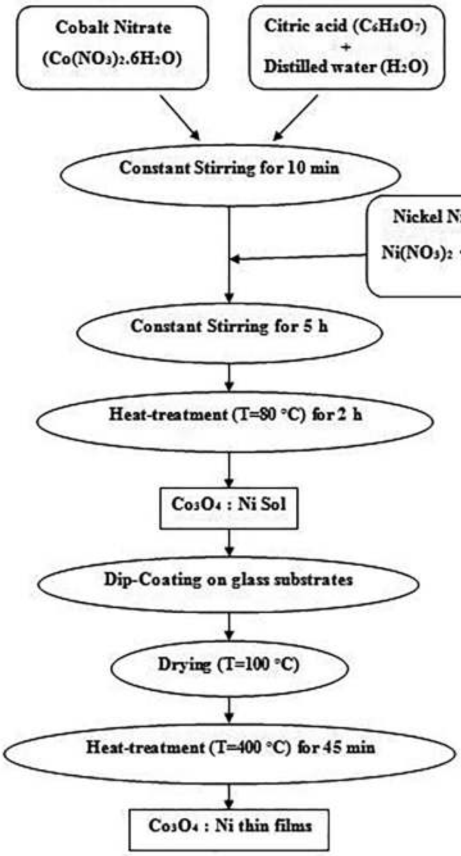

Figure 1. Schematic diagram of sol-gel process of Ni-doped Co_3O_4 preparation

Table 1. Optimized deposition parameters.

Dip coating parameters	Optimized values
Concentration of precursor	0.1 M
Volume of precursor	30ml
Solvent 100%	Citric acid
Relative humidity	40%
Substrate temperature	400 °C
Constant speed	5.0 Cm/min

2.3. Characterizations

The as-prepared samples were characterized by using different physical techniques. The optical transmittance spectra and band gap energies of Ni-doped Co_3O_4 thin films were measured using Shimadzu-1650 spectrophotometer in the wavelength range from 300 to 900 nm. The phase and crystal structure of all samples were studied by X-ray diffraction (Rigaku miniflex 600) with *CuKα* radiation (λ= 1.5406 Å). The vibrational behavior of the samples was investigated by FT-IR (Alpha Bruker spectrophotometer) in the wavenumber range from 400 to 4000 cm^{-1}. Impedance measurements were carried out using Agilent4284A LCR-meter operating in the frequency range 75 KHz to 20 MHz with an oscillation amplitude of 1V.

3. Results and discussion

3.1. Optical analysis

In this part, the UV-Vis spectra of Ni-doped Co_3O_4 films were recorded in the wavelength range from 300 to 900 nm. Fig.2 shows the optical transmission spectra of Ni-doped Co_3O_4 thin films. All the obtained spectra manifest the presence of two sharp absorption edges in the visible region, which are attributed to the ligand to metal charge transfer (LMCT) event of ($O^{-2} \rightarrow Co^{2+}$) and ($O^{-2} \rightarrow Co^{3+}$) in Co_3O_4. This indicates the presence of two energy band gaps, in agreement with the literature[17].

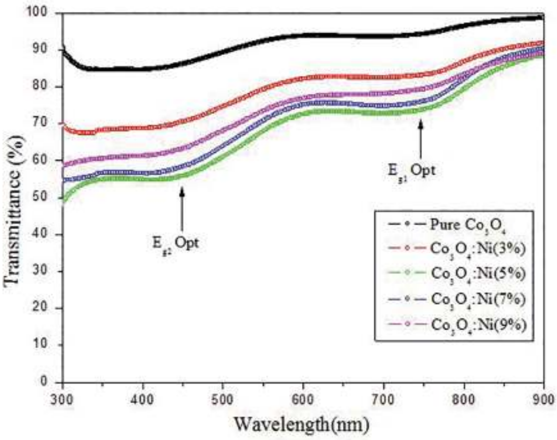

Figure 2. Transmittance spectra of pure and Ni-doped Co_3O_4 films

Fig.2 shows a high transmittance in the range of visible light (T ~ 85% for pure Co_3O_4 and between 60% and 75% is observed for all doped samples), attributed to a better structural homogeneity. It is well known that Co_3O_4, (i.e. $Co^{2+}[Co^{3+}]_2O_4$) has a normal spinel crystal structure, knowing that the Co^{2+} ions occupy the tetrahedral sites, while Co^{3+} ions occupy the octahedral sites[18]. Since the p states of O^{2-} ions are located closely to the d states of Co^{3+} ions, p electrons can easily undergo a transition. At low temperatures this peak splits and results in a doublet corresponding to $p(O^{2-}) \rightarrow e_g(Co^{3+})$ and p $(O^{2-}) \rightarrow t_2(Co^{2+})$. The higher band gap should be associated to the $O^{2-} \rightarrow Co^{2+}$charge transfer (valence to conduction band excitation) and the lower band gap associated to the $O^{2-} \rightarrow Co^{3+}$charge transfer (with the Co^{3+} level located below the conduction band)[19-21]. Jacques Pankove. I[22] suggest that the multiple band gap energy for the Co_3O_4 thin films may be due to the valence band degeneracy. Moreover, the electrical conduction of Co_3O_4 occurs by the hopping of small polarons between two different valency states of the cobalt ions[23]. A Schematic representation of the band structure of Pure Co_3O_4 is given in Fig.3. The variation of absorption coefficient against photon energy *hv* for direct band-to-band transition has the form of:

$$(\alpha h\upsilon) = A(h\upsilon - E_g)^x \qquad (1)$$

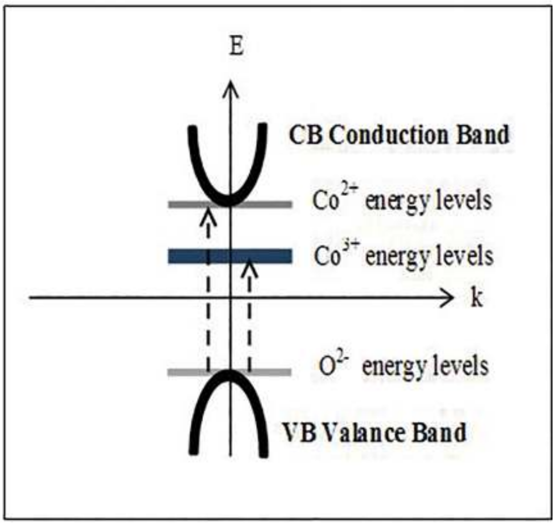

Figure 3. Schematic representation of the band structure of Co_3O_4

where α is the absorption coefficient $\left(\alpha = \frac{1}{d}\ln\left\{\frac{1}{T}\right\}\right)$, *hv* is the photon energy, E_g the band gap energy and *A* the edge parameter. The value of *x* is 2 for indirect allowed transitions and ½ for direct allowed transitions[24]. Fig.4 shows the plots of $(\alpha h\upsilon)^2$*vs* $(h\upsilon)$. The extrapolation of a straight portion to the energy axis at $\alpha = 0$ can give two values of band gap $E_{g1} = 1.50eV$ corresponds ($O^{-2} \rightarrow Co^{3+}$) and $E_{g2} = 2.20eV$ corresponds ($O^{-2} \rightarrow Co^{2+}$). Louardi et al.[24] have obtained the same results. The refractive index is calculated by Ravindra relation ship[25]:

$$n = 4.084 - 0.68(E_g) \qquad (2)$$

The film thickness d has been calculated from UV-visible data using the following equation[26]:

$$d = \frac{\lambda_1 \lambda_2}{2n(\lambda_1 - \lambda_2)} \qquad (3)$$

Where, *n* is the refractive index at two adjacent maxima or minima at wavelengths λ_1 and λ_2. Results obtained for the direct band gap energy, films' thickness and refractive index of our films at different doping levels are reported in Table 2. In Fig.5, we show the variations of the band gap energies as a function of doping level.

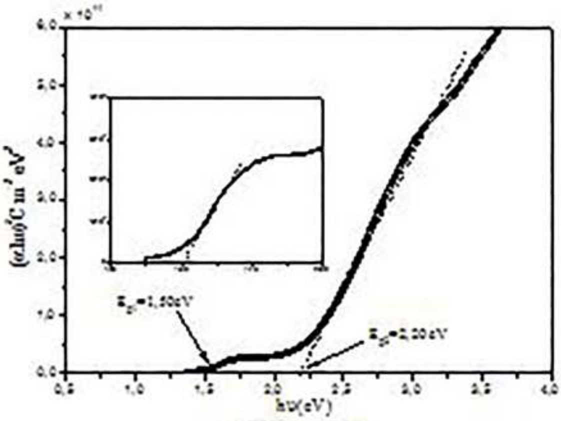

(a) Co_3O_4 Pure

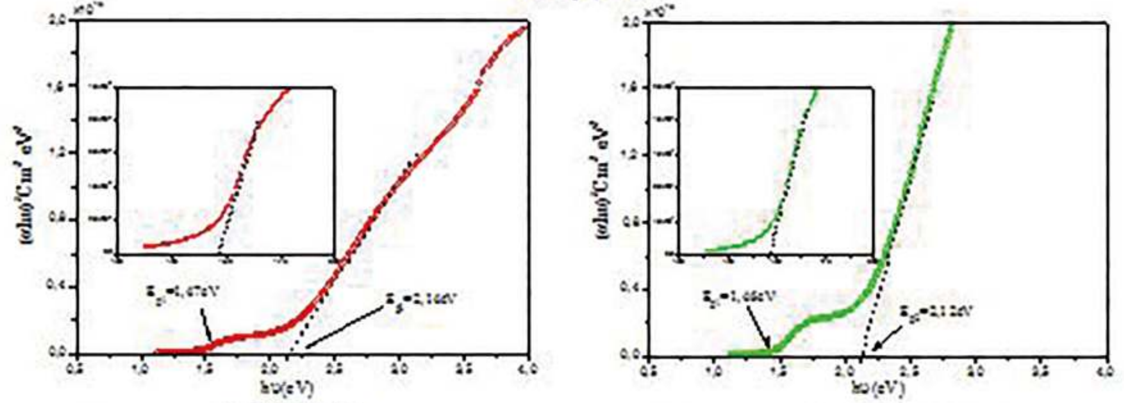

(b) Co_3O_4:Ni (3%)

(c) Co_3O_4:Ni (5%)

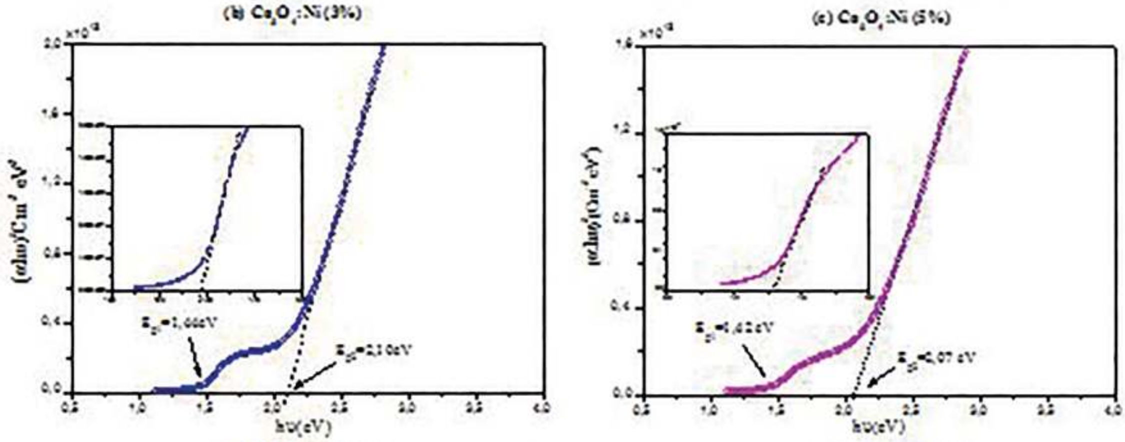

(d) Co_3O_4:Ni (7%)

(e) Co_3O_4:Ni (9%)

Figure 4. Plot of $(\alpha h v)^2$ versus hv of pure and Ni-doped Co_3O_4 films at different doping levels

Table 2. Band gap energy, thikness and refractive index of pure and Ni-doped Co_3O_4 films.

Sample	E_{g1} (eV)	E_{g2} (eV)	Thikness (nm)	Refractive index
Pure Co_3O_4	1.50	2.20	256.01	2.588
Co_3O_4: Ni (3%)	1.47	2.14	301.90	2.628
Co_3O_4: Ni (5%)	1.46	2.12	313.28	2.642
Co_3O_4: Ni (7%)	1.44	2.10	244.93	2.656
Co_3O_4: Ni (9%)	1.42	2.07	251.48	2.676

Ni-doped Co_3O_4 at different doping levels show slight decrease in the band gap compared to pure Co_3O_4 with the increase of doping levels (the lower band gap energy shifted from1.50 for pure Co_3O_4 and to 1.42 eV for the 9wt% Ni-doped Co_3O_4, the higher band gap energy shifted from 2.20 for pure Co_3O_4 and to 2.07 eV for the 9wt% Ni-doped Co_3O_4), This behavior may be due to the network distortions caused by the introduction of nickel ions in the Co_3O_4 matrix and the formation of impurity energy levels (acceptor level)

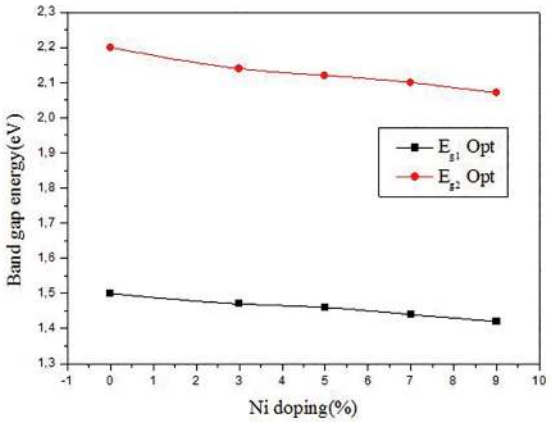

Figure 5. Variation of the optical gap of Ni-doped Co_3O_4 films at different doping levels

within the band gap. On the other hand nickel contributes to the creation of holes and increases its role by the number of charge carriers (holes) which contribute to the conductivity knowing that Co_3O_4 is a P type semiconductor.

Refraction index increases from 2.588 (pure) to 2.676 (9%Ni). This can be explained by the crystallization and the densification of the material. J.A.K. Tareen et al.[26] suggest that the Ni atoms are located in the octahedral sites of the spinel lattice. Moreover at the microscopic level, the increase of *n* refers to the modification of the polarizability of the ions and the local field in the material[27,28].

3.2. Structural analysis

The structural characterization of the powders was analyzed using Rigakuminiflex 600 Xray diffractometer with CuKα radiation in the 2θ range of 20-80°. Fig.6 shows the X-ray diffraction (XRD) pattern of Ni-doped Co_3O_4 powders after calcination in muffle furnace at 400°C for 3 hours. All obtained powders show multiple diffraction peaks coincided well with the cubic spinel type structure (*Fd3m* space group). The presence of reflection peaks associated to (220), (311), (222), (400), (422), (511) and (440) planes at 2θ = 31.27°, 36.88°, 38.62° 44.81°, 55.75°, 59.45°and 65.38° respectively, knowing that ⟨311⟩ as preferential orientation. No parasitic phase of nickel clusters, nickel oxides (NiO) or Ni-Co, (NiCoO3) oxide phases has been observed in the detection limit of the apparatus, which indicate a high purity of the samples. These results have been previously confirmed by several authors[20-29]. The crystalline phase of Ni-doped Co_3O_4 is identical to the Co_3O_4cubic spinel phase. When the Ni atoms introduced into the matrix it can either "substitute" or "interstice" in the lattice. The lattice spacing was calculated from the Bragg's cubic system formula[20]:

$$d_{(hkl)} = \frac{a}{\sqrt{(h^2+k^2+l^2)}} \tag{4}$$

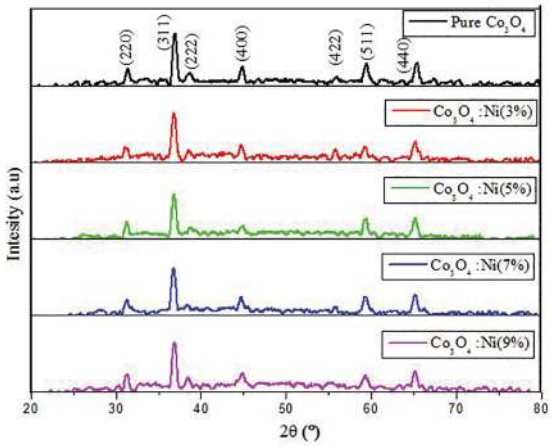

Figure 6. XRD patterns of pure and Ni-doped Co_3O_4 powders for different Ni-doping amounts

The particle sizes of Ni-doped Co_3O_4 samples were calculated using the full width at half maximum (FWHM) of (311) peak from the Debye-Scherrer formula[30], knowing that the width increases as the particle size decreases

$$D = \frac{0.9\lambda}{\beta\cos\theta} \tag{5}$$

Where D is the crystallite size, λ is the wavelength of the CuKα radiation (1.5406Å), β the full-width half maximum (FWHM) of Bragg peak observed at Bragg angle θ. It was found that the crystallite size of the samples was in the range of [214-279] Å. The values of D and β obtained are given in Table 3.

3.3. Infrared Spectroscopy

Fig.7, shows the FT-IR transmission spectra of Pure and Ni-doped Co_3O_4 films at different doping levels (3wt%, 5wt%, 7wt% and 9wt%), deposited by dip coating technique on silicon substrates and annealed at 400°C. In the investigated region 400-4000 cm^{-1}, all obtained spectra have two absorption bands υ_1, υ_2 at 565 cm^{-1} and 662 cm^{-1} assigned to the stretching vibration of metal-oxygen bond (Co-O or Ni-O) in Co_3O_4 spinel oxide with (*Fd3m* space group), Gomaa A et al.[23] have obtained the same results. The absorption band υ_1 at 565 cm^{-1} is associated with the OB_3 vibrations in the spinel lattice where B denotes the Co^{3+} ions in an octahedral hole. The second band υ_2 (662 cm^{-1}) is the ABO_3 vibration, where A denotes Co^{2+} ions in a tetrahedral hole. The absorption peak υ_4 at (2350 cm^{-1}), is assigned to the vibration of C=O bond[31]. The experimental values of absorption bands have been collected from different sources[12,17,32]. These observations are in good agreement with the XRD results (Fig.6).

Table 3. Structural parameters of pure and Ni-doped Co_3O_4 samples.

Samples	(hkl)	2θ	d spacing (Ǻ)	Lattice parameters (Ǻ)	FWHM (deg)	Crystallite size D (Ǻ)
Pure Co_3O_4	(311)	36.88	2.435	8.075	0.30	279
Co_3O_4: Ni (3%)	(311)	36.80	2.440	8.095	0.34	260
Co_3O_4: Ni (5%)	(311)	36.84	2.437	8.082	0.40	220
Co_3O_4: Ni (7%)	(311)	36.78	2.441	8.095	0.40	222
Co_3O_4: Ni (9%)	(311)	36.83	2.438	8.085	0.41	214

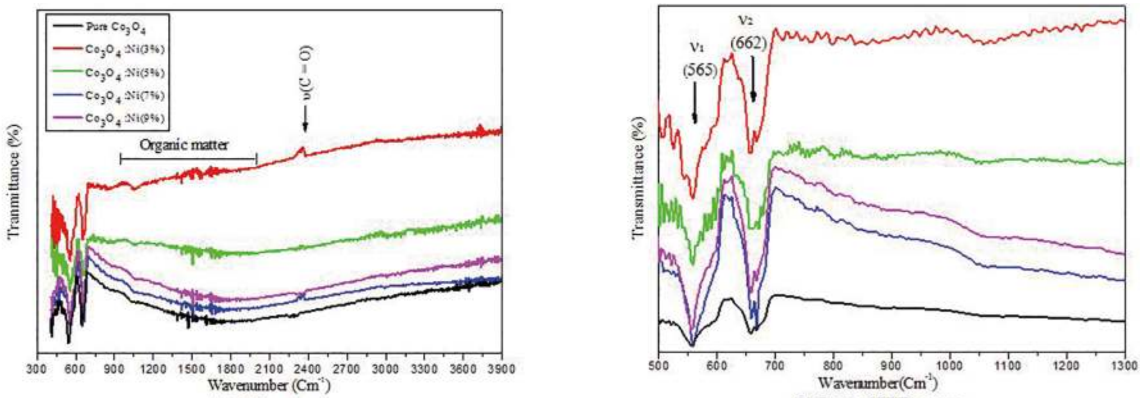

(a) FTIR spectra

(b) Zoom of FTIR spectra

Figure 7. FT-IR spectra of pure and Ni-doped Co_3O_4 films at different doping levels

3.4. Impedance spectroscopy

The measurement of the electrical properties of materials requires powerful tools to explore the electrical behavior, and that is through modeling them by an equivalent circuit[33]. In this method we apply a sinusoidal disturbance of constant amplitude and a variable frequency to determine the conduction properties of a polycrystalline oxide and also, in theory, the different contributions to the conduction of a material (grains, grain boundaries, Pores, defects)[16,30,34] It also characterizes the different electrically active regions in the material and demonstrates their existence by their individual electrical properties. The electrical behavior of our films described in terms of one of the four complex expressions[35], each consists of real and imaginary component.

Complex impedance:

$$Z^* = Z' + jZ'' = R_s - j/\omega C_s \tag{6}$$

Complex admittance:

$$Y^* = Y' - Y'' = \frac{1}{R_P} + j\omega C_p \tag{7}$$

Complex permittivity:

$$\varepsilon^* = \varepsilon' - j\varepsilon'' \tag{8}$$

Complex modulus:

$$M^* = M' + M'' \tag{9}$$

These expressions are interrelated as:

$$M^* = \frac{1}{\varepsilon^*} = j\omega C_0 Z^* = j\omega C_0\left(\frac{1}{Y^*}\right) \tag{10}$$

Where R_S and C_S are the series resistance and capacitance; R_P and C_P are the parallel resistance and capacitance, C_0 is the empty capacitance, $\omega=2\pi\upsilon$, where υ is the applied frequency and $j^2=-1$. Previous formalisms provide the opportunity to expand the scope to highlight a particular aspect of the electrical response of the sample. The idealized plot (Z" versus Z') that describes the electrical behavior of a polycrystalline oxide has three components, each of these components corresponds to a particular relaxation frequency. At higher frequencies, the component corresponds to the bulk properties (ν_b). At intermediate frequencies, the electrical behavior due to the grain boundaries (ν_{gb}) and at low frequencies the electrical response corresponds to electrode process (ν_{el}), or processes occurring in the material/electrode interface ($\nu_{el} \ll \nu_{gb} \ll \nu_b$)[36]. Several factors influence the electrical behavior of materials as chemical composition, impurities, ageing and conditions of preparation. The volume and grain boundary properties, chemical composition, impurities, ageing and preparation conditions make the actual oxide system rather complicated. The electrical characteristic of a material is shown by the appearance of semicircular arcs in the Nyquist plots. Fig.8 is the Nyquist representation of pure and Ni-doped Co_3O_4 thin films, whose f frequency varies from 75 kHz to 20 MHz at ambient temperature. The processes that occur in the electrode are modeled by an equivalent electrical circuit. The physical logic of the system indicates that the concurrent processes are connected in parallel. The capacity C_p of the thin films was calculated using the following equation:

$$C_P = \frac{1}{2\pi f_P R_p} \tag{11}$$

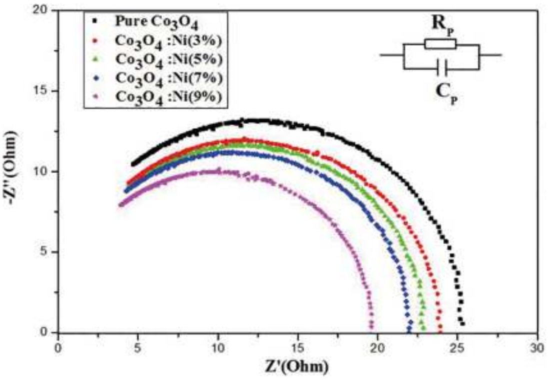

Figure 8. Nyquist plots of pure and Ni-doped Co_3O_4 thin films at different doping levels

The variation of the resistance and capacitance as a function of Ni doping level are listed in Table 4 and shown in Fig.9. It is clear that the resistance of cobalt oxide decreases and the capacity increases with the increase of doping level. This shift is also due to the introduction of nickel ions in Co_3O_4 lattice which induces a variation in the particle size and consequently introduce more grain boundaries within the samples. Two conduction mechanisms are simultaneously present, conduction across the grain and conduction through the grain boundaries. The effect of grain boundaries in samples becomes more dominant with respect to the contribution of the grains in the conduction mechanism.

Table 4. Values of *fc*, *Rp* and *Cp* of pure and Ni-doped Co_3O_4 films.

Samples	fc (MHz)	Rp (Ω)	Cp (nF)
Pure Co_3O_4	13.40	25.68	462
Co_3O_4: Ni (3%)	13.29	24.27	493
Co_3O_4: Ni (5%)	13.07	22.84	533
Co_3O_4: Ni (7%)	12.85	21.93	564
Co_3O_4: Ni (9%)	12.51	19.56	650

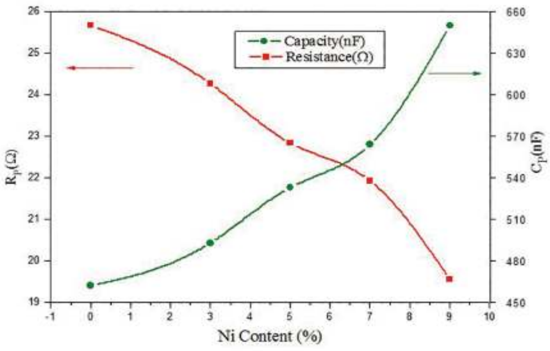

Figure 9. Variation of capacity and resistance of pure and Ni-doped Co_3O_4 as a function of Ni doping level

4. Conclusion

In conclusion, we have successfully synthesised Ni-doped cobalt oxide (Co_3O_4) thin films using a sol gel technique in order to investigate their optical, structural and electrical properties. X-ray diffraction patterns revealed that Ni-doped Co_3O_4 samples were crystallized in cubic spinel structure knowing that the crystallite size was found to be from 214 to 279 Å. The as synthesis films, exhibit a high transmission ~ 60-85% in the visible region. Optical studies concluded that Co_3O_4 has multiple band gap energies with direct transitions 2.20 eV ($O^{2-}\rightarrow Co^{2+}$) and 1.50 eV ($O^{2-}\rightarrow Co^{3+}$). The band gap energies of our samples were determined by the Tauc plot. The values of the band gaps were found to decrease as the dopant concentration increases, it might be due to the formation of acceptor level within the band gap. The FT-IR spectra of pure and Ni-doped Co_3O_4 films revealed two distinct bands that arise due to the stretching vibrations of the metal Co-O or Ni-O bonds in the investigated region. The FT-IR spectra were typical of a cubic spinel structure with space group *Fd-3m* and served as a clear evidence for the presence of cubic Co_3O_4 in agreement with X-ray diffraction results. The complex impedance spectroscopy indicates that the physical concurrent processes of Ni-doped Co_3O_4 are connected in parallel *RC*. The conduction mechanism of all samples is highly due to the grain boundaries.

5. References

1. Yao L, Xi Y, Xi G, Feng Y. Synthesis of cobalt ferrite with enhanced magnetostriction properties by the sol-gel-hydrothermal route using spent Li-ion battery. *Journal of Alloys and Compounds*. 2016;680:73-79. DOI: 10.1016/j.jallcom.2016.04.092

2. Razmi H, Habibi E. Amperometric detection of acetaminophen by an electrochemical sensor based on cobalt oxide nanoparticles in a flow injection system. *Electrochimica Acta*. 2010;55(28):8731-8737. DOI: 10.1016/j.electacta.2010.07.081

3. Shinde VR, Mahadik SB, Gujar TP, Lokhande CD. Supercapacitive cobalt oxide (Co_3O_4) thin films by spray pyrolysis. *Applied Surface Science*. 2006;252(20):7487-7492. DOI: 10.1016/j.apsusc.2005.09.004

4. Smith GB, Ignatiev A, Zajac G. Solar selective black cobalt: preparation, structure, and thermal stability. *Journal of Applied Physics*. 1980;51(8):4186-4196. DOI: 10.1063/1.328276

5. Patil PS, Kadam LD, Lokhande CD. Preparation and characterization of spray pyrolysed cobalt oxide thin films. *Thin Solid Films*. 1996;272(1):29-32. DOI: 10.1016/0040-6090(95)06907-0

6. Gulino A, Dapporto P, Rossi P, Fragalà I. A Novel Self-Generating Liquid MOCVD Precursor for Co_3O_4 Thin Films. *Chemistry of Materials*. 2003;15(20):3748-3752. DOI: 10.1021/cm034305z

7. Young RS, ed. *Cobalt: Its Chemistry, Metallurgy and Uses*. New York: Reinhold Publishing Corp.; 1960.

8. Armelao L, Barreca D, Gross S, Tondello E. Sol-Gel and CVD Co_3O_4 thin films characterized by XPS. *Surface Science Spectra*. 2001;8(1):14-23. DOI: 10.1116/11.20010601

9. Victoria SG, Raj AME, Ravidhas C. An insight in the structural, morphological, electrical and optical properties of spray pyrolysed Co_3O_4 thin films. *Materials Chemistry and Physics*. 2015;162:852-859. DOI: 10.1016/j.matchemphys.2015.07.015

10. Tang Q, Zhu H, Chen C, Wang Y, Zhu Z, Wu J, et al. Preparation and Characterization of Nanoscale Cobalt Blue Pigment for Ceramic Inkjet Printing by Sol-Gel Self-Propagating Combustion. *Materials Research*. 2017;20(5):1340-1344. DOI: 10.1590/1980-5373-MR-2017-0322

11. Patil V, Joshi P, Chougule M, Sen S. Synthesis and Characterization of Co_3O_4 Thin Film. *Soft Nanoscience Letters*. 2011;2(1):1-7. DOI: 10.4236/snl.2012.21001

12. Švegl F, Orel B, Grabec-Švegl I, Kaučič V. Characterization of spinel Co_3O_4 and Li-doped Co_3O_4 thin film electrocatalysts prepared by the sol-gel route. *Electrochimica Acta*. 2000;45(25-26):4359-4371. DOI: 10.1016/S0013-4686(00)00543-0

13. Chatelon JP, Terrier C, Bernstein E, Berjoan R, Roger JA. Morphology of SnO_2 thin films obtained by the sol-gel technique. *Thin Solid Films*. 1994;247(2):162-168. DOI: 10.1016/0040-6090(94)90794-3

14. Zarbali M, Göktaş A, Mutlu IH, Kazan S, Şale AG, Mikailzade F. Structure and Magnetic Properties of $La_{0.66}Sr_{0.33}MnO_3$ Thin Films Derived Using Sol-Gel Technique. *Journal of Superconductivity and Novel Magnetism*. 2012;25(8):2767-2770. DOI: 10.1007/s10948-011-1260-z

15. Göktas A. Sol-gel derived $Zn_{1-x}Fe_xS$ diluted magnetic semiconductor thin films: Compositional dependent room or above room temperature ferromagnetism. *Applied Surface Science*. 2015;340:151-159. DOI: 10.1016/j.apsusc.2015.02.115

16. Kharoubi A, Bouaza A, Benrabah B, Ammari A, Khiali A. Characterization of Ni-doped TiO_2 thin films deposited by dip-coating technique. *The European Physical Journal Applied Physics*. 2015;72(3):30301. DOI: 10.1051/epjap/2015150282

17. Kandalkar SG, Gunjakar JL, Lokhande CD, Joo OS. Synthesis of cobalt oxide interconnected flacks and nano-worms structures using low temperature chemical bath deposition. *Journal of Alloys and Compounds*. 2009;478(1-2):594-598. DOI: 10.1016/j.jallcom.2008.11.095

18. Thota S, Kumar A, Kumar J. Optical, electrical and magnetic properties of Co_3O_4 nanocrystallites obtained by thermal decomposition of sol-gel derived oxalates. *Materials Science and Engineering: B*. 2009;164(1):30-37. DOI: 10.1016/j.mseb.2009.06.002

19. Pal J, Chauhan P. Study of physical properties of cobalt oxide (Co_3O_4) nanocrystals. *Materials Characterization*. 2010;61(5):575-579. DOI: 10.1016/j.matchar.2010.02.017

20. Jacobs JP, Maltha A, Reintjes JGH, Drimal J, Ponec V, Brongersma HH. The Surface of Catalytically Active Spinels. *Journal of Catalysis*. 1994;147(1):294-300. DOI: 10.1006/jcat.1994.1140

21. Shelef M, Wheeler MAZ, Yao HC. Ion scattering spectra from spinel surfaces. *Surface Science*. 1975;47(2):697-703. DOI: 10.1016/0039-6028(75)90218-6

22. Pankove JI. *Optical Processes in Semiconductors*. Englewood Cliffs: Prentice-Hall; 1971.

23. Ali GAM, Fouad OA, Makhlouf SA. Structural, optical and electrical properties of sol-gel prepared mesoporous Co_3O_4/SiO_2 nanocomposites. *Journal of Alloys and Compounds*. 2013;579:606-611. DOI: 10.1016/j.jallcom.2013.07.095

24. Louardi A, Rmili A, Ouachtari F, Bouaoud A, Elidrissi B, Erguig H. Characterization of cobalt oxide thin films prepared by a facile spray pyrolysis technique using perfume atomizer. *Journal of Alloys and Compounds*. 2011;509(37):9183-9189. DOI: 10.1016/j.jallcom.2011.06.106

25. Ravindra NM. Energy gap-refractive index relation - some observations. *Infrared Physics*. 1981;21(5):283-285. DOI: 10.1016/0020-0891(81)90033-6

26. Tareen JAK, Malecki A, Doumerc JP, Launay JC, Dordor P, Pouchard M, et al. Growth and electrical properties of pure and Ni-doped Co_3O_4 single crystals. *Materials Research Bulletin*. 1984;19(8):989-997. DOI: 10.1016/0025-5408(84)90212-5

27. Goktas A, Aslan F, Tumbul A, Gunduz SH. Tuning of structural, optical and dielectric constants by various transition metal doping in ZnO:TM (TM=Mn, Co, Fe) nanostructured thin films: A comparative study. *Ceramics International*. 2016;43(1 Pt A):704-713. DOI: 10.1016/j.ceramint.2016.09.217

28. Goktas A, Mutlu IH. Structural, Optical, and Magnetic Properties of Solution-Processed Co-Doped ZnS Thin Films. *Journal of Electronic Materials*. 2016;45(11):5709-5720. DOI: 10.1007/s11664-016-4771-3

29. Santos GA, Santos CM, da Silva SW, Urquieta-González EA, Sartoratto PPC. Sol-gel synthesis of silica-cobalt composites by employing Co_3O_4 colloidal dispersions. *Colloids and Surfaces A: Physicochemical and Engineering Aspects*. 2012;395:217-224. DOI: 10.1016/j.colsurfa.2011.12.033

30. Benrabah B, Bouaza A, Kadari A, Maaref MA. Impedance studies of Sb doped SnO_2 thin film prepared by sol gel process. *Superlattices and Microstructures*. 2011;50(6):591-600. DOI: 10.1016/j.spmi.2011.08.009

31. Ammari A, Bellal B, Zebbar N, Benrabah B, Trari M. Thermal-frequency dependence study of the sub-band localized states effect in Sb-doped SnO_2 based sol-gel thin films. *Thin Solid Films*. 2017;632:66-72. DOI: 10.1016/j.tsf.2017.02.060

32. Makhlouf MT, Abu-Zied BM, Mansoure TH. Direct Fabrication of Cobalt Oxide Nanoparticles Employing Sucrose as a Combustion Fuel. *Journal of Nanoparticles*. 2013;2013:384350. DOI: 10.1155/2013/384350

33. Barsoukov E, Macdonald JR, eds. *Impedance Spectroscopy, Theory, Experiment, and Applications*. 2nd ed. New York: John Wiley & Sons; 2005.

34. Göktas A, Tumbul A, Aslan F. Grain size-induced structural, magnetic and magnetoresistance properties of $Nd_{0.67}Ca_{0.33}MnO_3$ nanocrystalline thin films. *Journal of Sol-Gel Science and Technology*. 2016;78(8):262-269. DOI: 10.1007/s10971-016-3960-0

35. McDevitt NT, Baun WL. Infrared absorption study of metal oxides in the low frequency region (700-240 cm^{-1}). *Spectrochimica Acta*. 1964;20(5):799-808. DOI: 10.1016/0371-1951(64)80079-5

36. Mechiakh R, Meriche F, Kremer R, Bensaha R, Boudine B, Boudrioua A. TiO_2 thin films prepared by sol-gel method for waveguiding applications: Correlation between the structural and optical properties. *Optical Materials*. 2007;30(4):645-651. DOI: 10.1016/j.optmat.2007.02.047